Available online at www.sciencedirect.com
ScienceDirect
Journal of Power Sources 160 (2006) 65–72
JOURNAL OF POWER SOURCES
www.elsevier.com/locate/jpowsour

Enhanced electrocatalytic performance for methanol oxidation of a novel Pt-dispersed poly(3,4-ethylenedioxythiophene)–poly (styrene sulfonic acid) electrode

Chung-Wen Kuo [a], Li-Ming Huang [a], Ten-Chin Wen [a,*], A. Gopalan [b]

[a] *Department of Chemical Engineering, National Cheng Kung University, Tainan 70101, Taiwan*
[b] *Department of Industrial Chemistry, Alagappa University, Karaikudi, India*

Received 10 December 2005; received in revised form 7 January 2006; accepted 11 January 2006
Available online 5 June 2006

Abstract

A new catalyst electrode was prepared in which Pt particles were homogeneously distributed into a poly(3,4-ethylenedioxythiophene)–poly(styrene sulfonic acid) (PEDOT–PSS) matrix. Catalytic activity and stability for the oxidation of methanol were studied by using cyclic voltammetry and chronoamperometry. For comparative purposes, bulk Pt and PEDOT–PSS based electrodes were fabricated and tested. Enhanced electrocatalytic activity toward the oxidation of methanol was noticed when Pt particles were embedded into the PEDOT–PSS matrix. A high catalytic current for methanol oxidation (2.51 mA cm^{-2}) was found for the PEDOT–PSS–Pt electrode in comparison to bulk Pt electrode (0.45 mA cm^{-2}) at +0.6 V (versus Ag/AgCl). The enhanced electrocatalytic activity might be due to the dispersion of Pt particles into the PEDOT–PSS matrix and the synergistic effects between the dispersed Pt particles and the PEDOT–PSS matrix. The morphology and crystalline behavior of PEDOT–PSS–Pt and simple ITO/Pt films were determined by X-ray diffraction (XRD) analysis and scanning electron microscopy (SEM) and correlated with the enhanced electrocatalytic activity for the Pt-dispersed PEDOT–PSS electrode.

Keywords: PEDOT–PSS–Pt composite films; Electrooxidation; Methanol; Fuel cell; Electrocatalytic properties

1. Introduction

In the context of fast depletion of fossil fuel resources, research activities on batteries and full cells have been triggered. Among several types of fuel cells, polymer electrolyte based direct methanol fuel cells (DMFCs) are being projected for a variety of applications ranging from micro-power to mega-power devices [1–4]. The attractive features of DMFCs are due to a high theoretical energy density expected from methanol [5]. Furthermore, the fabrication of regenerative DMFCs, which is based on the concept of electrochemical reduction of CO_2 to CH_3OH and employing the latter as the fuel, seems to be interesting as this is also relates to the global warming problem [3].

Despite of the advantages and interesting aspects involved in using methanol as a fuel for electrochemical energy conversion, the need for better electrocatalysts has become inevitable. Extensive studies made on electrooxidation of methanol have clearly revealed that Pt metal can be an effective electrocatalyst for the process [6]. However, intermediate products of the reaction, like CO, are strongly absorbed at the electrode surface, which can subsequently restrict the electrocatalytic activity of electrode [7]. On the other hand, the increasing use of Pt may raise the price of Pt and deplete a scarce resource.

Two possible approaches were tried to circumvent the problem of using Pt in DMFCs and related applications. In a straightforward approach, bi- or tri-metallic catalysts involving transition metals were attempted [8]. In another approach, a few electrodes that exhibited enhanced electrocatalytic activities in comparison with the bulk-form of metal electrodes toward oxidation of small organic molecules have been fabricated through incorporation of transition metal particles into conducting polymer matrices [9–13].

In the present study, we have loaded Pt particles into a 3D-random matrix of a composite comprising a conduct-

* Corresponding author. Tel.: +886 6 2385487; fax: +886 6 2344496.
E-mail address: tcwen@mail.ncku.edu.tw (T.-C. Wen).

0378-7753/$ – see front matter © 2006 Elsevier B.V. All rights reserved.
doi:10.1016/j.jpowsour.2006.01.100

ing polymer, poly(3,4-ethylenedioxythiophene) (PEDOT) and poly(styrene sulfonic acid) (PSS). PEDOT has been attracting interest due to its high compatibility with other materials, very good film forming properties, high stability, high conductivity, and high extent of doping [14,15]. PEDOT doped with an excess of PSS, designated as PEDOT–PSS, is commercially available as a stable aqueous dispersion. Ghosh and Inganas [14] reported that PEDOT–PSS is a non-stoichiometric poly-electrolyte complex of PEDOT and PSS, with an excess of the latter component. Colloidal particles of PEDOT–PSS are negatively charged and expected to serve as a matrix for loading smaller particles of Pt through steric and electrostatic stabilization mechanisms [16–18]. Furthermore, the network structure of PEDOT–PSS has the resemblance of Nafion. PEDOT–PSS provides three dimensional (3D) reaction zones and increases the active surface area of Pt particles while in contact with the electrolyte. The presence of anionic dopants in PEDOT–PSS generates a pathway for protonic species and hence possesses suitable characteristics for DMFCs applications. Motivated by the above characteristics for PEDOT–PSS, we have developed a new type of electrode material incorporating Pt particles into a PEDOT–PSS matrix for application in DMFCs.

In this work, Pt particles were embedded into the PEDOT–PSS matrix by electrochemical deposition. PEDOT–PSS with its network structure acts as a three-dimensional, random and electronically conducting template (microreactor) and allows the formation of relatively uniform Pt particles. Performance characteristics of the Pt-loaded PEDOT–PSS matrix as a electrocatalyst toward the oxidation of methanol were monitored by using cyclic voltammetry and chronoamperometry. A comparison of catalyst performance between pristine Pt and PEDOT–PSS–Pt based electrodes was made. Also, morphological changes between the electrodes fabricated with indium tin oxide (ITO) as the substrate, ITO/Pt and ITO/PEDOT–PSS–Pt electrodes were compared using a scanning electron microscope (SEM) and X-ray diffraction (XRD) analysis, respectively.

2. Experimental

PEDOT–PSS (Alfa, 1.34 wt.%) matrix electrode (ITO/PEDOT–PSS) was prepared by spin coating (2000 rpm for 1 min) of a PEDOT–PSS thin film over the surface of ITO. Pt particles were deposited onto the ITO/PEDOT–PSS from a solution of H_2PtCl_6. For a comparative purposes, Pt particles were deposited onto simple ITO electrodes under otherwise similar conditions to the deposition of Pt particles onto ITO/PEDOT–PSS. Typically, a plating solution consisting of 5 mM $H_2PtCl_6{\cdot}H_2O$, 0.01 M HCl, and 0.1 M KCl (pH 1.96) was used. Cyclic voltammetry (CV) was employed to deposit Pt particles by cycling the potentials (versus Ag/AgCl) between −0.25 and 0.8 V for 30, 60, 90 and 120 cycles with a scan rate of 50 mV s^{-1}. After Pt particle incorporation, the electrode was rinsed with double distilled water for 5 min and dried at 150 °C for 3 min. The amount of Pt particles loaded onto the ITO/PEDOT–PSS or deposited onto ITO was calculated from the following equation:

$$m = \frac{Q_{\text{dep}} M}{FZ}$$

where amount (m) was calculated by using the charge (Q_{dep}) (obtained through graphical integration of cyclic voltammetric curves) utilized for the deposition of Pt particles. M is the atomic weight of Pt, F is the Faraday constant, and Z is the number of electrons transferred (taken as four for the formation of Pt). Electrochemical characterizations of composite electrodes were performed using a PGSTAT 20 electrochemical analyzer, AUTOLAB Electrochemical Instrument (The Netherlands). All experiments were carried out in a three-component cell. An Ag/AgCl electrode (in 3 M KCl), Pt wire and ITO coated glass plate (1 cm^2 area) were used as reference, counter and working electrodes, respectively. A Luggin capillary, whose tip was set at a distance of 1–2 mm from the surface of the working electrode, was used to minimize errors due to iR drop in the electrolytes.

The surface morphology was observed with a scanning electron microscopy (Philips X1-40 FEG). X-ray diffraction patterns of ITO/PEDOT–PSS–Pt composite and ITO/Pt films were collected by exposing the samples to Siemens D5000 X-ray source with Cu Kα (1.542 Å) as a target in the diffraction angles (2θ) ranged from 20° to 80° with scan rate 4° min^{-1}.

3. Results and discussion

3.1. Growth of Pt particles embedded in PEDOT–PSS

Cyclic voltammetry was employed for the deposition of Pt particles into the PEDOT–PSS film. For comparative purposes, Pt particles were also deposited onto a ITO electrode. Fig. 1 represents the cyclic voltammograms (CVs) recorded during the growth of Pt particles embedded into (a) PEDOT–PSS and (b) deposited onto bare ITO (without PEDOT–PSS) from a solution of 5 mM H_2PtCl_6. Reduction of Pt^{4+} to Pt^0 has been reported to be at ∼0.5 V [19]. However, current responses corresponding to Pt metal deposition were also found at more negative potentials [20]. An increasing trend in the cathodic current with an increasing number of potential cycles was noticed for the potentials positive to 0.2 V at the cathodic sweep. This signifies the deposition of Pt metal particles onto ITO or embedding of Pt particles into the PEDOT–PSS matrix during the application of potentials. Interestingly, peaks corresponding to the adsorption–desorption of hydrogen could be noticed only with the ITO/PEDOT–PSS–Pt electrode in contrast to a bare ITO/Pt electrode. This indicates that Pt particles are well dispersed in the PEDOT–PSS matrix [19].

Also, there exists a difference in the amount of Pt particles (deposited/incorporated) between the ITO electrode and ITO/PEDOT–PSS electrodes. Fig. 2 represents the plot of charge utilized for Pt particle deposition/insertion (a measure of amount of deposit) versus number of cycles. Fig. 2 shows that Pt particle incorporation into the PEDOT–PSS matrix occurred with two different rates of incorporation. The plot, charge versus number of potential cycles, which represents the rate of deposition of Pt particles into PEDOT–PSS composite, shows a chang-

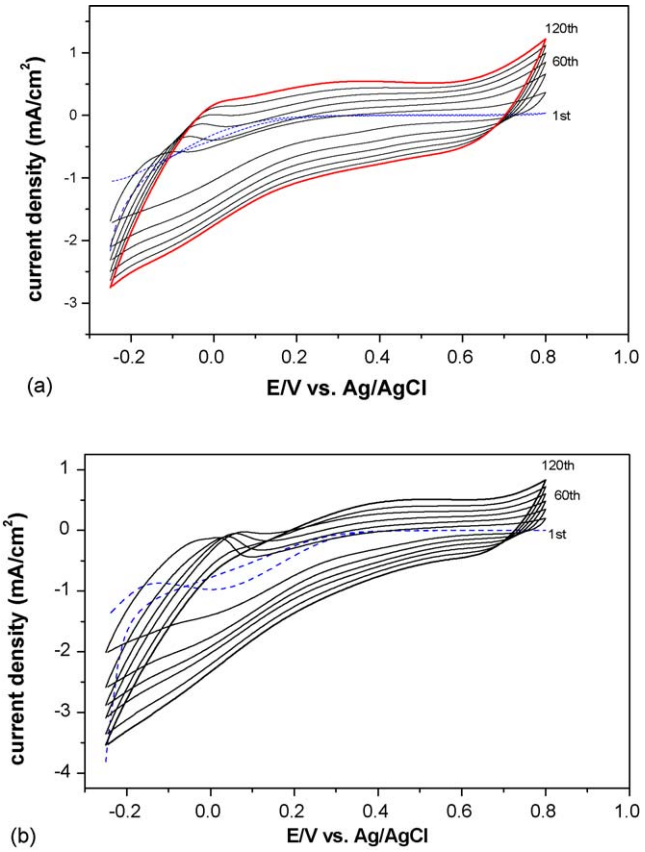

Fig. 1. Consecutive CVs recorded during the incorporation of Pt particles into (a) PEDOT–PSS matrix and deposition of Pt particles onto (b) ITO electrode from a solution of 5 mM $H_2PtCl_6 \cdot H_2O$, 0.01 M HCl, and 0.1 M KCl. Cyclic voltammetry was carried out at a scan rate of 50 mV s^{-1} in the potential range from −0.25 to +0.8 V for 120 cycles.

ing slope in the two regions. A rapid increase in growth rate was observed during the initial 30 cycles. Also, higher growth rate for Pt particles incorporation was evident for the composite than for the deposition of Pt particles onto a simple ITO electrode. The higher growth rate for Pt particle incorporation into

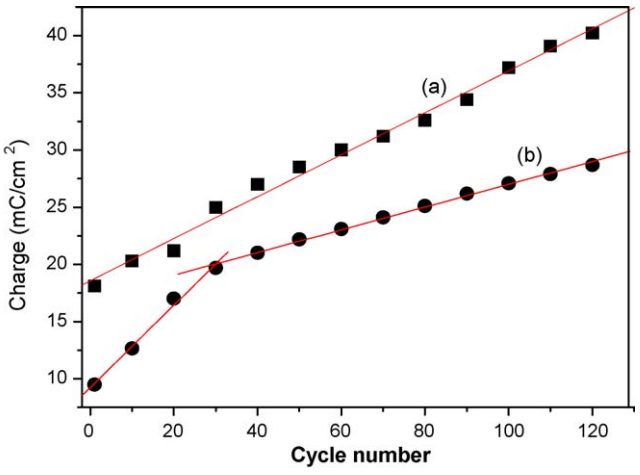

Fig. 2. Dependence of the charge utilized for deposition/incorporation of Pt particles (Q_G) on the number of potential cycles while forming (a) ITO/Pt and (b) ITO/PEDOT–PSS–Pt composite electrodes.

ITO/PEDOT–PSS–Pt during the initial 30 cycles may be due to a combination of the several factors. Firstly, the porous and rough morphology of PEDOT–PSS [21] and presence of SO_3^- groups allow an increased uptake of Pt^{4+} ions. The higher growth rate noticed for the initial cycles of potential (Fig. 2b) arises from the loading of Pt^{4+} ions within the pores of the PEDOT–PSS and consequent reduction to Pt particles. During subsequent cycles (beyond 30), Pt particles were formed over the Pt particle-filled sites of PEDOT–PSS. This happens in the second stage and is inferred from the lower slope of the plot of charge versus number of cycles (Fig. 2). This signifies a comparatively lower growth rate in the second stage. In contrast to this type of two-stage growth behavior, a single stage increase in growth rate was observed for the deposition of Pt particles onto the ITO electrode. In the case of deposition of Pt particles onto the ITO electrode, the smoothness of the surface of ITO resulted in the formation of aggregates of Pt particles. The matrix of PEDOT–PSS loaded with Pt particles was a good adherent film on the surface of ITO. In contrast, film of Pt particles deposited onto ITO was not stable due to poor adhesion with the ITO surface. Hence, PEDOT–PSS acts as a binder to provide contact for Pt particles with the ITO substrate.

3.2. Morphology of Pt particles embedded in the PEDOT–PSS matrix

Pt particles dispersed in the polymer matrix (PEDOT–PSS) exhibit interesting catalytic properties [22–26] because of the larger number of catalytic sites. The composite electrode offers few other advantages. It could be possible to recover the catalyst and recycle it wherever necessary. Also, the polymer matrix acts as a protective layer for the Pt nanoparticles and prevents aggregation of particles. We are reporting here the advantages of using PEDOT–PSS in tailor-designing the properties of Pt particles formed within the PEDOT–PSS matrix and the utility of Pt nanoparticles loaded in ITO/PEDOT–PSS for DMFC applications.

Fig. 3 shows the difference in the morphology between ITO/PEDOT–PSS–Pt and ITO/Pt surfaces. Pt particles were loaded into the PEDOT–PSS matrix by cyclic voltammetry (30 and 90 cycles). Pt particles deposited onto the surface of simple ITO exist as aggregates (Fig. 3a). Whilst, Pt particles are homogenously distributed onto the surface of ITO/PEDOT–PSS (Fig. 3b). Larger sized Pt particles were incorporated within PEDOT–PSS when loaded with higher number of cycles (Fig. 3c). The larger Pt particles are also homogeneously distributed into the PEDOT–PSS matrix (Fig. 3c).

Fig. 4 shows the spatial distribution of Pt particles in the ITO/PEDOT–PSS and simple ITO. A higher active surface area was noticed for the Pt particles dispersed in the PEDOT–PSS matrix. Fig. 4 shows a schematic of the distribution of Pt particles in the simple ITO and ITO/PEDOT–PSS and explains the reason for the homogenous distribution of Pt particles in the PEDOT–PSS matrix. Pt particles deposited on the surface of simple ITO are tightly packed and hence a portion of the active surface area of Pt particles may not be available due to the tight packing with other particles. On the other hand, PEDOT–PSS

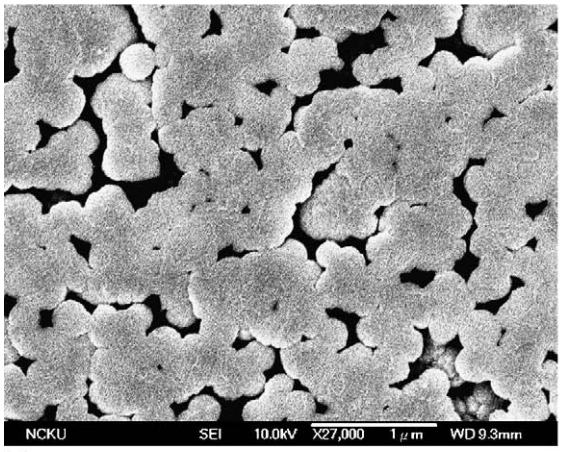

(a)

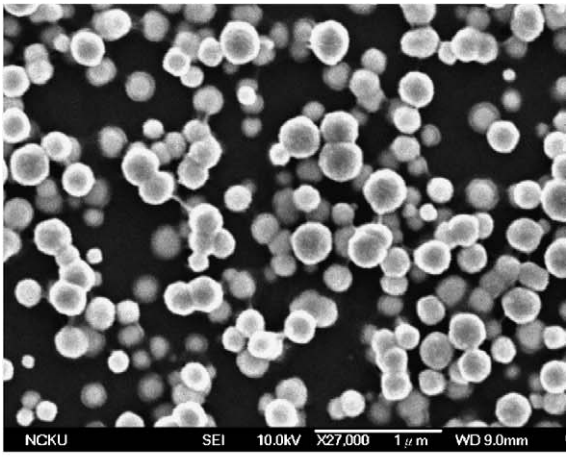

(b)

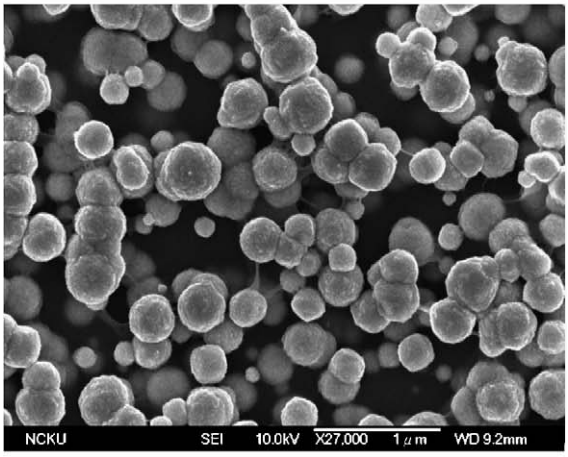

(c)

Fig. 3. SEM images for (a) ITO/Pt, (b) ITO/PEDOT–PSS–Pt (growth of Pt for 30 cycles) and (c) ITO/PEDOT–PSS–Pt (growth of Pt for 90 cycles) electrodes.

provides an environment to disperse the individual Pt particles and keeps the active surface area a maximum. We anticipate that PEDOT–PSS–Pt having such a morphology for Pt particles is more suitable for use in DMFC applications. It should be remembered that Pt particles could not be dispersed on carbon black supports while using the catalyst in DMFCs applications. Hence, the requirements for optimal inter-particle spacing for

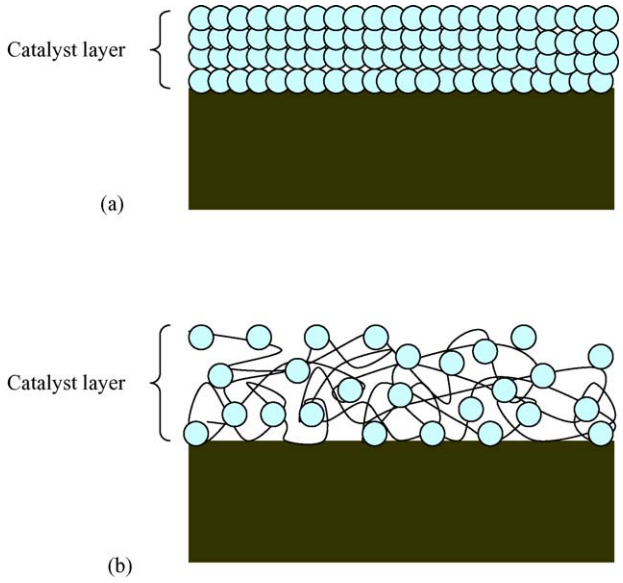

Fig. 4. Schematic representation of (a) conventional anode structure of bulk Pt electrode and (b) proposed anode structure of Pt particles embedded in PEDOT–PSS matrix.

rapid methanol diffusion could not be met. Ultimately, the catalytic efficiencies of Pt particles in such an environment were low. Hence, we hypothesize that the catalyst, Pt particles dispersed in PEDOT–PSS, may show better catalytic characteristics for DMFC applications. We have also observed that Pt particles dispersed in the PEDOT–PSS matrix possess a different crystal structure and hydrogen adsorption capability in comparison to Pt particles deposited onto simple ITO.

3.3. Crystal structure of Pt particles incorporated into the PEDOT–PSS matrix

The crystalline structure of Pt particles incorporated onto the ITO/PEDOT–PSS matrix was examined by XRD analysis. XRD patterns of ITO/PEDOT–PSS–Pt (30 cycles), ITO/PEDOT–PSS–Pt (90 cycles) are compared with XRD patterns of ITO/PEDOT–PSS and ITO/Pt (Fig. 5). The XRD pattern of ITO/PEDOT–PSS (Fig. 5a) shows weak patterns at $2\theta \sim 30^\circ$, 35° and 50°. Diffraction peaks corresponding to Pt (1 1 1), Pt (2 0 0) and Pt (2 2 0) can be clearly seen at $2\theta = 40^\circ$, 46° and 68°, respectively, for the Pt particles deposited onto simple ITO (Fig. 5b). Fig. 5c and d present the diffraction patterns of ITO/PEDOT–PSS–Pt having Pt particles loaded with different numbers of cycles in cyclic voltammetric experiments. The diffraction peaks corresponding to Pt and PEDOT–PSS can be clearly noticed. Pt particles embedded into the PEDOT–PSS matrix shows a polycrystalline structure. Strikingly, (1 1 1) and (2 0 0) peaks show a difference in intensities for Pt particles deposited with different numbers of cycles in PEDOT–PSS–Pt. This is attributed to the increase in the primary particle size with the increase in number of cycles used for Pt deposition [27]. The increase in (2 2 0) and (1 1 1) peak intensities also suggests an increase in the amount of crystalline phase in Pt particles.

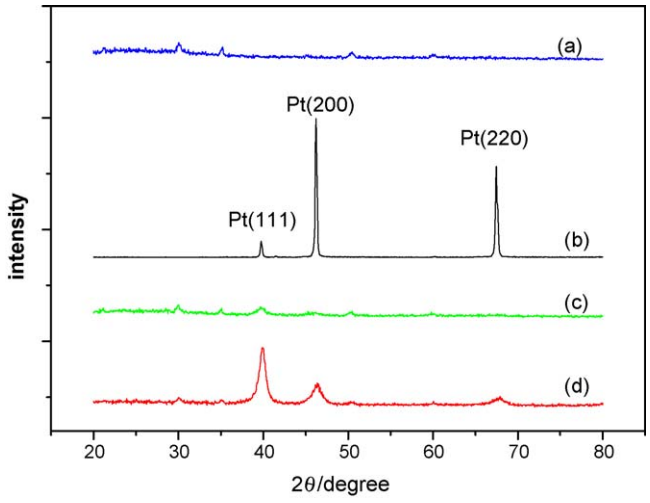

Fig. 5. XRD spectra of (a) PEDOT–PSS, (b) bulk Pt, (c) PEDOT–PSS–Pt (growth of Pt for 30 cycles) and (d) PEDOT–PSS–Pt (growth of Pt for 90 cycles) electrodes.

3.4. Hydrogen adsorption characteristics for ITO/PEDOT–PSS–Pt

Films of Pt particles deposited onto simple ITO were not stable due to poor adhesion with the surface of ITO. Hence, instead of ITO/Pt, we have used bulk Pt electrode for the comparative evaluation of ITO/PEDOT–PSS–Pt with the ITO/Pt electrode toward voltammetric behavior in 0.5 M H_2SO_4. In further electrochemical experiments, we have used bulk Pt electrode instead of ITO/Pt electrode. Cyclic voltammograms (CVs) of ITO/PEDOT–PSS, ITO/PEDOT–PSS–Pt and bulk Pt electrodes recorded with a scan rate of 50 mV s^{-1} in 0.5 M H_2SO_4, are presented in Fig. 6. The CV pattern of bulk Pt electrode is consistent with the CV curve of polycrystalline Pt electrode reported by Paulus et al. [28]. In the potential region between −0.2 and +0.2 V (V versus SCE), the responses corresponding to hydrogen adsorption/desorption were noticed with an accompanying bisulfate adsorption/desorption. As can be seen in Fig. 6, bulk Pt and ITO/PEDOT–PSS–Pt electrodes have similar hydrogen adsorption/desorption characteristics. In contrast, a large background current without hydrogen adsorption/desorption peak was witnessed at ITO/PEDOT–PSS electrode (Fig. 6, insert). There is a difference in current density of hydrogen desorption between bulk Pt and PEDOT–PSS–Pt electrodes. It is known that the integrated intensity of hydrogen desorption represents the number of sites of Pt available for hydrogen adsorption and desorption [28–30]. Charges for hydrogen desorption on the electrode surfaces were calculated by assuming a constant double-layer charging current over the whole potential range. The charge for hydrogen desorption on the PEDOT–PSS–Pt surface was 2.99 mC cm^{-2}, which is five times larger than that on the bulk Pt surface (0.587 mC cm^{-2}). This is reminiscent of a much higher active surface area for PEDOT–PSS–Pt electrodes and consistent with the well-dispersed morphological environment for Pt particles in the PEDOT–PSS matrix (as shown in Fig. 3a). Besides that, in the cathodic sweep, a peak at 0.4 V was observed for ITO/PEDOT–PSS–Pt, and is assigned to the

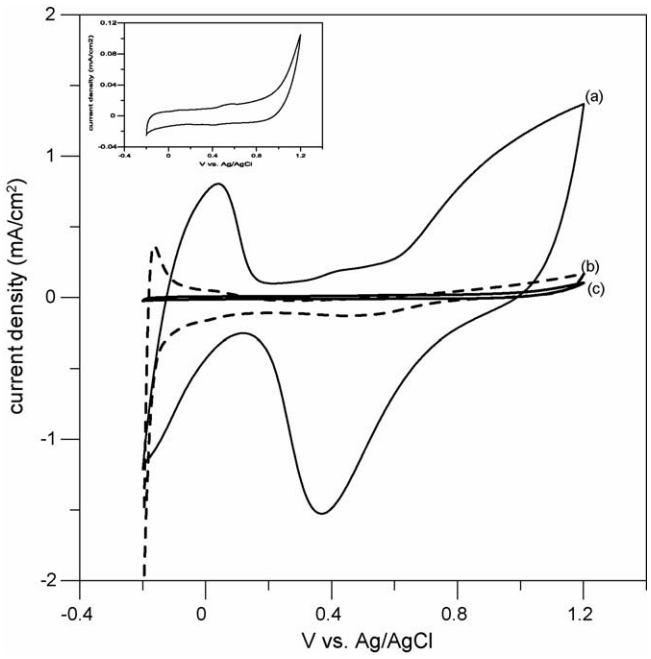

Fig. 6. Cyclic voltammograms of (a) ITO/PEDOT–PSS–Pt, (b) bulk Pt and (c) PEDOT–PSS electrodes in 0.5 M H_2SO_4 at the potential range from −0.2 to +1.2 V with a scan rate = 50 mV s^{-1}. The insert is bare PEDOT–PSS.

reduction of PtO to metallic Pt. Indeed, the PEDOT–PSS film behaves as a good probe for the deposition of Pt particles and increases the density of the active sites on the electrode surface.

3.5. Electrocatalytic activity and stability of PEDOT–PSS–Pt for methanol oxidation

The catalytic activities of ITO/PEDOT–PSS–Pt, and ITO/PEDOT–PSS composite electrodes were evaluated and compared with bulk Pt electrode (instead of using non-adherent ITO/Pt electrode) toward electrooxidation of methanol (Fig. 7). Clearly, ITO/PEDOT–PSS did not have the electrocatalytic properties for methanol oxidation (Fig. 7c). On the other hand, ITO/PEDOT–PSS–Pt showed current response similar to the published literature [32]. At the bulk Pt electrode, the current for the methanol oxidation increased slowly below 0.4 V in the anodic sweep (Fig. 7, insert). This is due to the formation of reaction intermediates [31,32]:

$$CH_3OH + Pt \rightarrow Pt\text{–}(CH_ZO)_{ad} + (4 - Z)H^+ + (4 - Z)e^- \quad (0 \leqq Z \leqq 4) \quad (1)$$

The current increases quickly and reaches a peak at around +0.6 V. This is ascribed to the partial oxidation of surface Pt, which helps in the transformation of intermediates to carbon dioxide:

$$Pt + H_2O \rightarrow Pt\text{–}OH + H^+ + e^- \quad (2)$$

$$Pt\text{–}(CH_ZO)_{ad} + (2 + Z)Pt\text{–}OH \rightarrow (2 + Z)Pt + CO_2 + (1 + Z)H_2O \quad (0 \leqq Z \leqq 4) \quad (3)$$

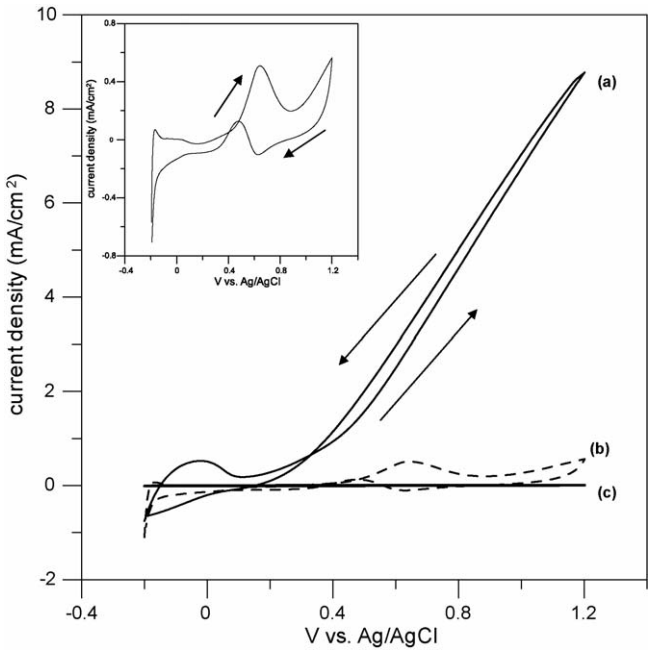

Fig. 7. Cyclic voltammograms of (a) ITO/PEDOT–PSS–Pt, (b) bulk Pt and (c) PEDOT–PSS electrodes in 0.1 M CH_3OH + 0.5 M H_2SO_4 at the potential range from −0.2 to +1.2 V with a scan rate = 50 mV s^{-1}. The insert is bulk Pt electrode.

On the cathodic sweep, the peak corresponds to methanol adsorption occurs at a less negative potential (0.5 V) than noticed on the forward sweep (0.6 V). This can be ascribed to the presence of fresh Pt surface available from the reduction of Pt oxide during the negative sweep.

Cyclic voltammetric studies of methanol oxidation at Pt electrodes revealed that the electrooxidation could occur over a wide potential range depending on the electrode characteristics [33,34]. Studies of methanol oxidation also showed that the extent of the catalytic effects may be dependent on the amount and structural peculiarities of the Pt deposits and also on the distribution of Pt particles. We have noticed oblique line-like current responses for methanol oxidation with the ITO/PEDOT–PSS–Pt electrode. The electrode showing such an oblique curve signifies a higher electroactivity for methanol oxidation. We have made a comparison of the peak currents at the peak potentials corresponding to methanol oxidation for the ITO/PEDOT–PSS–Pt and Pt electrode [35]. A comparison of the CVs for methanol oxidation on ITO/PEDOT–PSS–Pt (Fig. 7a) and bulk Pt (Fig. 7b) show that a significantly higher oxidation current was witnessed for the ITO/PEDOT–PSS–Pt electrode (Fig. 7a). For example, a current value of 2.51 mA cm^{-2} was noticed at 0.6 V in the positive sweep for ITO/PEDOT–PSS–Pt. However, a current value of 0.45 mA cm^{-2} was noticed for the bulk Pt electrode. It is obvious that the enhanced catalytic activity for methanol oxidation in the case of ITO/PEDOT–PSS–Pt arises from the more active surface area of Pt particles embedded into the PEDOT–PSS matrix. The reasons for the improvement of catalytic activity of Pt embedded in PEDOT–PSS are presented here.

Firstly, a high surface area for Pt particles is anticipated due to the uniform distribution of Pt particles into the three-dimensional conducting PEDOT–PSS matrix. The results with methanol oxidation, as observed by us, suggest that the enhanced catalytic activities for Pt particles loaded into PEDOT–PSS may be due to the amount and the structural peculiarities of the micro-deposits of Pt and their distribution in the polymer matrix (PEDOT–PSS). Previous reports revealed that the structure of catalyst particles and the distribution of particles within the matrix of conducting polymers have shown a dependence on the efficiencies of the oxygen reduction reaction [36]. We also anticipate that PEDOT–PSS may act as a stabilizer for Pt particles and prevent aggregation of Pt particles. Also, an enhanced stability for Pt particles is anticipated as the result of steric and electrostatic stabilization of Pt particles provided by PEDOT–PSS. As a result, smaller Pt particles were formed. The above view is supported by the following reports [37–39]. Dalmia et al. [37] have demonstrated the feasibility of synthesizing nanometer-sized Pt colloids using a negatively charged polymer, poly(*N*-sulfonatopropyl *p*-benzamide). Ahmadi et al. [38,39] have reported the synthesis of nanometer-sized Pt colloids using polyacrylic acid and the effect of the polymer concentration on the shape of Pt particles.

Our ultimate intention in fabricating ITO/PEDOT–PSS–Pt electrode was to explore the possibility of using the catalyst electrode in DMFC applications. The limitations that are normally encountered in the use of Pt particles in DMFC applications motivated us to use a PEDOT–PSS–PT electrode to circumvent some of the limitations. The limitation of using Pt particles in DMFCs is reviewed briefly here. The main issue that limits the practical application of DMFCs is the low activity of the anodic catalysts and the crossover of methanol from anode to cathode. The latter is caused by the concentration difference between anode and cathode and can be diminished by using a low methanol concentration as well as using a modified proton exchange membrane. The former is caused by the self-poisoning of the catalysts. Catalysis by Pt particles is required for the oxidation of organic molecules. However, the intermediates formed during the oxidation of methanol, such as CO_{ad} act as poisons [40]. In this context, it is to be noted that use of polymer matrix to embed Pt particles can avoid these drawbacks. Polymers may influence the electrooxidation of small organic molecules [41]. The polymer may: (1) hinder the formation of strongly absorbed poisonous species; (2) catalyze the oxidation of strongly adsorbed poisonous species; and (3) catalyze the oxidation of weakly-adsorbed poisonous species.

Our results using the catalyst, ITO/PEDOT–PSS–Pt for electrooxidation of methanol indicated that the poisoning is minimized. PEDOT–PSS matrix acts as a good substrate for the deposition of Pt particles, and increases the density of the active sites on the electrode surface. Ultimately, the PEDOT–PSS film improves significantly the efficiency of the Pt particles catalyst, producing a considerable increase in the anodic current for methanol oxidation (Fig. 7a).

ITO/PEDOT–PSS–Pt electrodes also exhibited a minimum catalyst poisoning. Chronoamperometric responses at

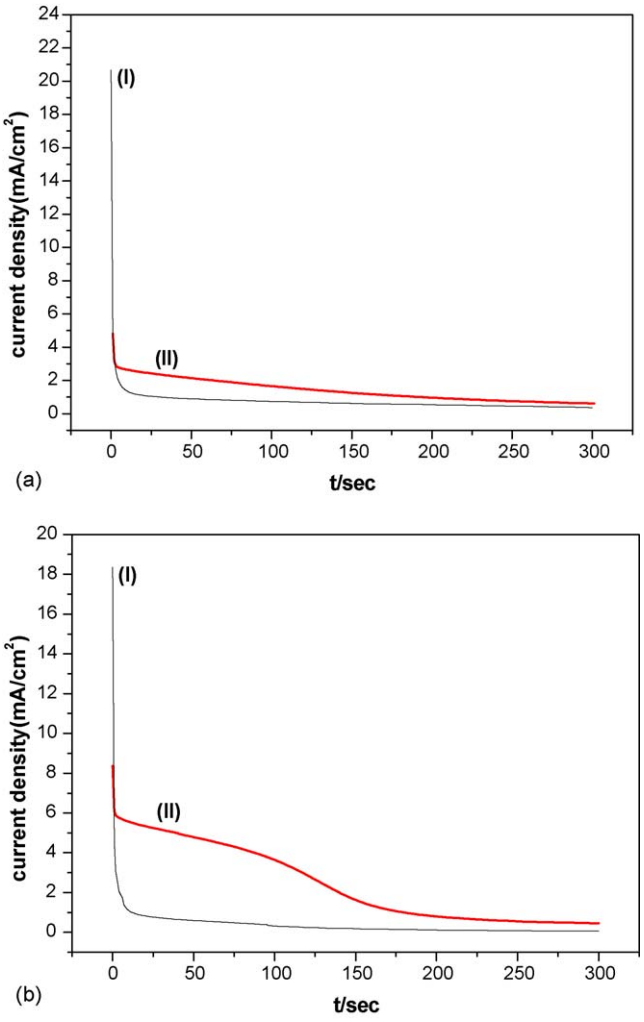

Fig. 8. Chronoamperometric response of (I) bulk Pt and (II) PEDOT–PSS–Pt at (a) 0.6 and (b) 0.8 V (versus Ag/AgCl) in 0.1 M CH_3OH + 0.5 M H_2SO_4 solution.

ITO/PEDOT–PSS–Pt and Pt electrodes with a solution of 0.1 M CH_3OH in 0.5 M H_2SO_4 were recorded at 0.6 and 0.8 V (Fig. 8a and b) and compared to evaluate the catalyst poisoning effect by these electrodes. In each of the potential step experiments, an initial potential (E_1) of 0.0 V was set for 30 s. At this potential, formation of CO on the electrode surface is more probable. The potential was then increased and kept at E_2 (0.6 V) for 5 min to reach a constant current value at the potential. At 0.6 V, ITO/PEDOT–PSS–Pt shows its higher catalytic properties toward the methanol oxidation in comparison to bulk Pt electrode. For example, the current at 150 s is 1.25 mA cm^{-2} for ITO/PEDOT–PSS–Pt and 0.62 mA cm^{-2} at the bulk Pt electrode. Upon setting E_2 as 0.8 V, ITO/PEDOT–PSS–Pt still showed a higher current density (1.63 mA cm^{-2}) in comparison with bulk Pt electrode (0.19 mA cm^{-2}). However, a decrease in steady-state current density was noticed for both the electrodes. This might be due to the formation of oxide and consequent diminishing of the number of sites available for methanol oxidation [30].

4. Conclusions

Pt particles were successfully embedded into a PEDOT–PSS matrix to form a PEDOT–PSS–Pt film. The composite, PEDOT–PSS–Pt, based electrode proved to be a promising material as a catalyst for methanol oxidation. The electrode having Pt particles embedded into PEDOT–PSS showed a significantly higher current for methanol oxidation. The matrix of PEDOT–PSS provided a suitable environment for dispersing Pt particles without aggregation, which is evident from the SEM results. Also, the PEDOT–PSS matrix may provide a pathway for proton migration in DMFC applications. The enhanced electrocatalytic activity of Pt in PEDOT–PSS opens up the possibility to use a lesser amount of Pt in catalyst fabrication for fuel cell applications.

Acknowledgement

The financial support of this work by the National Science Council of Taiwan under NSC-94-2214-E-006-010 is gratefully acknowledged.

References

[1] N.M. Markovic, T.J. Schmidt, V. Stamenkovic, P.N. Ross, Fuel Cell 1 (2001) 105.
[2] A.K. Shukla, R.K. Raman, Annu. Rev. Mater. Res. 33 (2003) 155.
[3] S.K. Mondal, R.K. Raman, A.K. Shukla, N. Munichandraiah, J. Power Sources 145 (2005) 16.
[4] A. Hamnett, in: R.G. Compton, G. Hancock (Eds.), Chemical Kinetics, vol. 37, Elesiver, Amsterdam, 1999, p. 593.
[5] R. Parson, T. Vander Noot, J. Electroanal. Chem. 257 (1988) 1.
[6] T. Iwasita, Electrochim. Acta 47 (2002) 3663.
[7] H. Wang, T. Loffler, H. Baltruschat, J. Appl. Elctrochem. 31 (2001) 759.
[8] T.R. Ralph, M.P. Hogarth, Platinum Met. Rev. 46 (2002) 117.
[9] B. Rajesh, K.R. Thampi, J.-M. Bonard, A.J. McEvoy, N. Xanthopoulos, H.J. Mathieu, B. Viswanathan, J. Power Sources 133 (2004) 155.
[10] D. Profeti, P. Olivi, Electrochim. Acta 49 (2004) 4979.
[11] L.H. Mascaro, D. Goncalves, L.O.S. Bulhoes, Thin Solid Films 461 (2004) 243.
[12] S.M. Golabi, A. Nozad, J. Electroanal. Chem. 521 (2002) 161.
[13] L. Niu, Q. Li, F. Wei, X. Chen, H. Wang, J. Electroanal. Chem. 544 (2003) 121.
[14] S. Ghosh, O. Inganas, Adv. Mater. 11 (1999) 1214.
[15] L. Adamczyk, P.J. Kulesza, K. Miecznikowski, B. Palys, M. Chojak, D. Krawczyk, J. Electrochem. Soc. 152 (2005) E98.
[16] Z. Qi, P.G. Pickup, Chem. Commun. 1 (1998) 15.
[17] A.B.R. Mayer, J.E. Mark, J. Polym. Sci. A 35 (1997) 3151.
[18] A.A. Antipov, G.B. Sukhorukov, Y.A. Fedutik, J. Hartmann, M. Giersig, H. Mohwald, Langmuir 18 (2002) 6687.
[19] L. Niu, Q. Li, F. Wei, S. Wu, P. Liu, X. Cao, J. Electroanal. Chem. 578 (2005) 331.
[20] K. Bouzek, K.-M. Mangold, K. Juttner, Electrochim. Acta 46 (2000) 661.
[21] F. Blanchard, B. Carre, F. Bonhomme, P. Biensan, H. Pages, D. Lemordant, J. Electroanal. Chem. 569 (2004) 203.
[22] A.B.P. Mayer, Polym. Adv. Technol. 12 (2001) 96.
[23] N. Toshima, T. Yonezawa, New J. Chem. (1998) 1179.
[24] N. Toshima, Y. Shiraishi, T. Teranishi, M. Miyake, T. Tominaga, H. Watanabe, W. Brijoux, H. Bonnemann, G. Schmid, Appl. Organomet. Chem. 15 (2001) 178.
[25] M. Lin, W. Yu, H. Lin, T. Zheng, J. Colloid Interf. Sci. 214 (1999) 231.
[26] J.-H. Choi, K.-W. Park, H.-K. Lee, Y.-M. Kim, J.-S. Lee, Y.-E. Sung, Electrochim. Acta 48 (2003) 2781.

[27] W. Sugimoto, H. Iwata, K. Yokoshima, Y. Murakami, Y. Takasu, J. Phys. Chem. B 109 (2005) 7330.
[28] U.A. Paulus, A. Wokaun, G.G. Scherer, T.J. Schmidt, V. Stamenkovic, N.M. Markovic, P.N. Ross, Electrochim. Acta 47 (2002) 3787.
[29] T.J. Schmidt, H.A. Gasteiger, G.D. Stab, P.M. Urban, D.M. Kolb, R.J. Behm, J. Electrochem. Soc. 145 (1998) 2354.
[30] A. Chen, D.J.L. Russa, B. Miller, Langmuir 20 (2004) 9695.
[31] R. Parsons, T. Vander Noot, J. Electroanal. Chem. 257 (1988) 9.
[32] W. Li, J. Lu, J. Du, D. Lu, H. Chen, H. Li, Y. Wu, Electrochem. Commun. 7 (2005) 406.
[33] M. Umeda, M. Kokubo, M. Mohamedi, I. Uchida, Electrochim. Acta 48 (2003) 1367.
[34] N.M. Arkosic, H.A. Gasteiger, P.N. Ross Jr., Electrochim. Acta 40 (1995) 91.
[35] Z.D. Wei, S.H. Chan, J. Electroanal. Chem. 569 (2004) 23.
[36] A. Yassar, J. Roncali, F. Garnier, J. Electroanal. Chem. 255 (1988) 53.
[37] A. Dalmia, C.L. Lineken, R.F. Savinell, J. Colloid Interf. Sci. 205 (1998) 535.
[38] T.S. Ahmadi, Z.L. Wang, T.C. Green, A. Henglein, M.A. Elsayed, Science 272 (1996) 1924.
[39] T.S. Ahmadi, Z.L. Wang, A. Henglein, M.A. Elsayed, Chem. Mater. 8 (1996) 1161.
[40] T.D. Jenvi, E.M. Stuve, in: J. Lipkowsi, P.N. Poss (Eds.), Electrocatalysis, Wiley, New York, 1998, p. 75.
[41] V.E. Kazarinov, V.N. Andreev, M.A. Spitsyn, A.P. Mayorov, Electrochim. Acta 35 (1990) 1459.